




Cite this: *RSC Adv.*, 2024, 14, 30192

# A facile strategy for the preparation of polylactide nano-microspheres with enhanced stereo-complexations

Ming Hua,<sup>†</sup> Ying Pan,<sup>†</sup> Changmei Jiang, Peiyan Yu, Xingang Li, Yao Gao, Sijun Xu  and Gangwei Pan \*

Stereo-complexed polylactide (sc-PLA) nano-microspheres were separated by adding poor solvent to the poly(L-lactide) (PLLA)/poly(D-lactide) (PDLA) blend solution. The effects of different process parameters (concentration, processing method, ratio of PLLA/PDLA blend solution to poor solvent) on the microsphere particle size were investigated. The microscopic morphology, crystallinity, and thermal properties were investigated by Fourier transform infrared spectroscopy, differential scanning calorimetry, two-dimensional wide-angle X-ray diffraction, transmission electron microscopy and scanning electron microscopy. The results indicated that when the concentration reached 10 wt% and the PLLA/PDLA blend solution to poor solvent ratio was 1 : 5, the sc-PLA nano-microspheres exhibited more regular shape, good sphericity and uniform particle size, and the highest crystallinity. Additionally, the degree of crystallinity of the stereo-complexed crystals was as high as 39.60%, the rate of stereo-complexation was 99.65%, and the melting temperature reached 220 °C, indicating notable improvement in the crystallization and thermal properties. The sc-PLA nano-microspheres obtained in this research could be used as a nucleating agent for fibers and drug delivery carrier, and the sc-PLA nano-microspheres have broad application prospects in the textile and biomedical fields.

Received 8th July 2024  
Accepted 12th September 2024

DOI: 10.1039/d4ra04919e

rsc.li/rsc-advances

## 1 Introduction

With growing concerns about global warming and the resulting increase in plastic pollution, the demand for biodegradable plastics has increased significantly.<sup>1</sup> Among the various biodegradable plastics, polylactide (PLA), a synthetic polyester derived from lactic acid,<sup>2–5</sup> has emerged as a particularly promising candidate due to its excellent processing, good biocompatibility<sup>6</sup> and mechanical properties.<sup>7–9</sup> However, despite these advantages, PLA still has its limitations in application. One of the key challenges associated with PLA is its inherent lack of flexibility and narrow processing window in practical applications,<sup>10,11</sup> which can lead to limitations in its applications. Additionally, PLA is susceptible to thermal degradation and hydrolysis,<sup>12,13</sup> which can affect its durability and stability. Several experimental studies have demonstrated that stereo-complexed polylactide (sc-PLA) is driven by the intensive intermolecular hydrogen(H)-bonding and dipole–dipole interactions between the enantiomeric molecular chains of poly(L-lactide) (PLLA) and poly(D-lactide) (PDLA).<sup>14</sup> Compared to homochiral PLA (hc-PLA), the incorporation of sc-PLA into

the system not only increases the melting temperature by 50 °C,<sup>15–17</sup> but also exhibits excellent crystallization rate and crystallinity, resulting in enhanced thermal stability and mechanical strength,<sup>18–26</sup> thus compensating for the shortcomings of PLA, which is brittle and has poor thermodynamic properties.<sup>27–29</sup>

Currently, researchers have found that microspheres exhibit size-dependent and surface-dependent properties, which are highly advantageous for a range of applications, including pharmaceuticals, food safety testing, medical diagnosis, sewage treatment and other advanced industrial manufacturing. In particular, PLA microspheres are optimal carriers for the controlled release of drugs in the field of drug formulation. When the active ingredients are loaded into the hollow or porous nano-microsphere carriers, the drugs are released at a slow rate in the human body. This approach reduces the toxicity of the drug and its negative effects, while increases drug efficacy.<sup>30</sup> Porous microspheres composed of magnetic materials can be employed as carriers for targeted drug delivery systems. The application of an external magnetic field can facilitate the delivery of anticancer drugs to a specific area, thereby enhancing the efficacy of immunomagnetic microspheres in targeting cancer cells.<sup>31</sup> Consequently, the preparation of nano-sized sc-PLA microspheres is of great significance in the field of PLA microsphere applications.

National & Local Joint Engineering Research Center of Technical Fiber Composites for Safety and Protection, School of Textile and Clothing, Nantong University, Nantong 226019, China. E-mail: pangangwei@ntu.edu.cn

<sup>†</sup> Ming Hua and Ying Pan contributed equally to this work.



Currently, the most common preparation methods of sc-PLA microspheres are emulsification solvent volatilisation,<sup>32</sup> spray drying,<sup>33</sup> electrospraying,<sup>34</sup> melting,<sup>35,36</sup> interfacial deposition,<sup>37,38</sup> supercritical fluid method,<sup>39</sup> high-pressure injection,<sup>40</sup> microfluidics and phase separation.<sup>41–43</sup> Nevertheless, those methods remain constrained by several factors. For instance, the high equipment and cleaning requirements of spray drying and microfluidic methods render them impractical for large-scale production. Similarly, the high temperature process used to prepare the melt method is incompatible with the encapsulation of temperature-sensitive drugs. Additionally, the electrospray technology is challenging for large-scale factory production. Furthermore, the emulsification solvent evaporation method exhibits a low encapsulation rate and a complex production process, and large-scale production necessitates constant adjustment of the process parameters. The principle of preparing microspheres by phase separation method is to add a poor solvent phase to the organic solution of the polymer to reduce the solubility of the polymer. The organic solution of the polymer is gradually extracted by the poor solvent, causing the polymer to undergo phase separation and solidification to form microspheres. Therefore, the addition of a poor solvent is crucial.

In addition, the advantages of preparing microspheres by the phase separation method are twofold. Firstly, no expensive experimental equipment is required and it is easy to set up the experimental equipment in the laboratory. Secondly, the phase separation method is conducive to the formation of microspheres for hydrophilic drugs. However, there are drawbacks to the preparation of microspheres by the phase separation method. A large number of organic solvents are used in the preparation process, and it is relatively difficult to remove the organic solvents from the final product. The microspheres produced by phase separation tend to aggregate, making large-scale production difficult.

Z. Feng *et al.*<sup>44</sup> extensively demonstrated a one-step microfluidic preparation process based on phase separation to generate triple-phase Janus microspheres with different degradation properties. The phase separation method plays a crucial role in this process. The specific preparation process of the phase separation method is as follows: the dispersed phase with specific components and the continuous phase are injected into the microfluidic chip, and the dispersed phase is sheared into droplets at the flow focusing sheath and flows into the winding channel to undergo solvent evaporation and phase separation. As the solvent evaporates, the increase in polymer concentration triggers liquid–liquid phase separation and a Janus structure is formed by spinodal decomposition and Ostwald ripening. Due to the potential cytotoxicity of PLGA, which can release toxic monomers or other cell-damaging by-products during degradation, the choice of PLA as a coating material is a relatively cautious one. However, PLA's poor thermal stability limits its use at high temperatures, and sc-PLA compensates for this by having a melting point that is 50 °C higher than that of PLA. Therefore, further research is needed to produce recyclable sc-PLA nanomicrospheres with high stereo-complex

crystallinity and high heat resistance by a simple phase separation method.

In view of the problems, this research proposes a facile method for the preparation of sc-PLA nano-microspheres. This involves the separation of sc-PLA nano-microspheres by the addition of a poor solvent phase to the PLLA/PDLA blend. Furthermore, the effects of different process parameters (concentration, the effects of treatment and the ratio of the blend to the poor solvent) on the morphology, crystallinity, and thermal properties of the nano-microspheres were investigated. This research provides a method and idea for the application of sc-PLA nano-microspheres in the textile and biomedical fields.

## 2 Experimental materials and methods

### 2.1. Experimental materials

The PLLA (6202D, with a weight average molecular weight of  $1.6 \times 10^5$ ) was purchased from Nature Works, and PDLA (with a weight average molecular weight of  $1.2 \times 10^5$ ) were synthesized by ring opening polymerization in a vacuum environment at 150 °C in the laboratory. Chloroform (CHL) was purchased from Ling Feng Chemical Reagent Co. Methanol (MT) was purchased from Ling Feng Chemical Reagent Co. All chemicals were of analytical grade and thus suitable for direct use without further purification.

### 2.2. Preparation of sc-PLA nano-microspheres

PLLA and PDLA were placed in a vacuum drying oven and dried at a constant temperature of 60 °C for 24 hours. PLLA and PDLA with a mass ratio of 1:1 were taken and dissolved in CHL solvent at a concentration of 2 wt%, 6 wt%, 10 wt% and 14 wt%, respectively, and placed in a magnetic stirrer at a certain rotational speed. Once dissolution was complete, the two bottles of the co-mixed solution were continued to be stirred for 2 hours to make a PLLA/PDLA blend solution. Phase separation were achieved by adding the blend solution to MT solution to obtain sc-PLA precipitate, which was then centrifuged at 5000 rpm for 15 minutes. The precipitate and solvent were poured into a Petri dish wrapped with tinfoil. Subsequently, the samples were placed in a vacuum drying oven at 60 °C, after vacuum drying for 24 hours the sc-PLA nano-microspheres powder was obtained. The powder was sampled and bagged. The preparation process was as shown in Fig. 1.

The nomenclature of the samples is as follows: SC – solution concentration – treatment – the ratio of the blend to the poor solvent. For example, when the concentration is 10%, the phase separation solution is prepared using static treatment, with the ratio of the PLLA/PDLA blend solution to the poor solvent is 1/10. The sample is recorded as SC-10-A-1/10. Following the application of low-speed stirring at 500 rpm, the samples are labeled as SC-10-C-1/10. Similarly, when subjected to medium-speed stirring at 1000 rpm, the samples are designated as SC-10-B-1/10. Pure PLA sample is recorded as PLA.



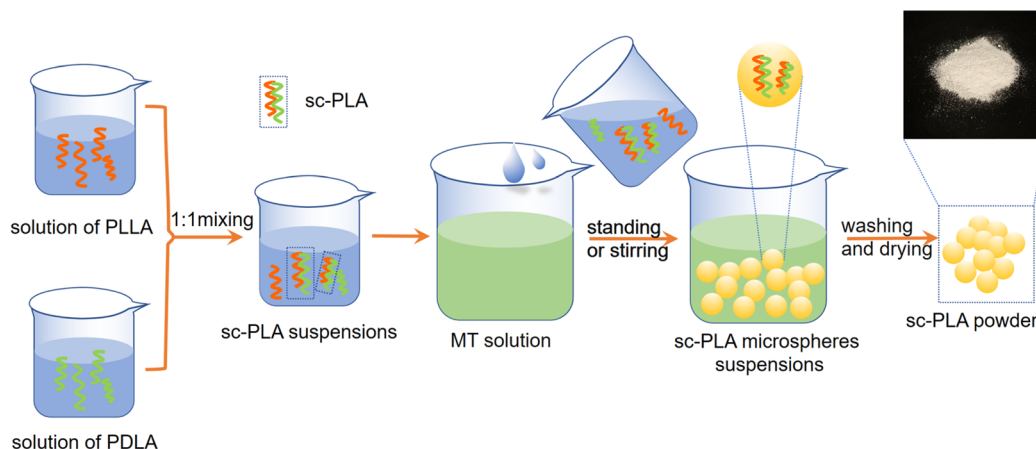


Fig. 1 Preparation process of sc-PLA nano-microspheres.

### 2.3. Characterization

The microscopic morphology and microsphere size of the sc-PLA nano-microspheres were observed using a Gemini SEM 300 scanning electron microscope (SEM). Subsequently, the nano-microspheres were subjected to infrared spectroscopy (FTIR) analysis using a Becto 33 FTIR spectrometer from Bruker, Germany. A Genesis XM type X-ray diffractometer (XRD) was used to determine the proportion of sc-PLA in the overall crystal. The XRD graphs were analyzed by the Jade software in order to estimate the degree of homo-crystallites ( $X_{c,H}$ ) and the degree of sc-crystallites ( $X_{c,S}$ ). The  $X_{c,H}$  represents the percentage of the homo-crystallites diffraction peaks' area to the total area of diffraction peaks and the  $X_{c,S}$  represents the percentage of the sc-crystallites diffraction peaks' area to the total area of diffraction peaks. The crystallinity of stereo-complexed crystals was expressed as the percentage of the diffraction peak area of stereo-complexed crystals to the total area of diffraction peaks. To gain insight into the thermal properties of the nano-microspheres, differential scanning calorimetry (DSC) analysis was conducted using a differential scanning calorimeter model 200 F3 from Netsch, Germany. The DSC testing method is as follows: Under the protection of a nitrogen flow rate of  $50 \text{ ml min}^{-1}$ , the temperature is first raised from  $20^\circ\text{C}$  to  $250^\circ\text{C}$  at a rate of  $20^\circ\text{C min}^{-1}$  to eliminate the thermal history. Then, the temperature is decreased from  $250^\circ\text{C}$  to  $20^\circ\text{C}$ . Finally, the temperature is increased again to  $250^\circ\text{C}$ . The second heating curve is recorded and analyzed. To measure the solvent resistance of the sc-PLA nano-microspheres, the sc-PLA was first immersed in CHL for 24 hours, then dispersed in a MT solution, and finally uniformly dropped on a copper mesh to allow the solvent to evaporate fully before being observed under Talos F200X TEM-type high-resolution transmission electron microscopes and SEM for morphological analysis.

To further quantify the crystallinity, the XRD curves were calculated and analyzed by Jade software to find out.

The crystallinity was calculated as follows:

$$X_{c,H}(\%) = \frac{S_{hc}}{S_{sc} + S_{hc} + S_a} \quad (1)$$

$$X_{c,S}(\%) = \frac{S_{sc}}{S_{sc} + S_{hc} + S_a} \quad (2)$$

where  $S_{hc}$ ,  $S_{sc}$  and  $S_a$  are the diffraction peak area of the homo-chiral, stereo-complexation and amorphous area.

The rate of stereo-complexation was calculated as follows:

$$\text{Rate of stereo-complexation}(\%) = \frac{X_{c,S}(\%)}{X_{c,H}(\%) + X_{c,S}(\%)}$$

## 3 Results and discussion

### 3.1. Morphologies and structures of the sc-PLA nano-microspheres

To determine the appropriate solution concentration for sc-PLA nano-microspheres, three kinds of sc-PLA nano-microspheres with different concentrations (2 wt%, 6 wt%, and 10 wt%) were prepared. Fig. 2 shows that sc-PLA nano-microspheres appeared at the three different solution concentrations. As the concentration decreased, the diameter of sc-PLA nano-microspheres became smaller and reached the nanometer level. The surface of sc-PLA nano-microspheres exhibited an uneven and grooved structure, as observed in Fig. 2b. This was attributed to the incomplete hardening of the nano-microspheres' interior, with the surface hardening first during the production process. The presence of wrinkles on the surface of sc-PLA nano-microspheres indicates the collapse of the outer hard shell as the inner portion hardens. Comparing the three concentrations, it is evident that sc-PLA nano-microspheres (SC-10-A-1/10) produced by the phase separation method exhibit a more regular shape, good sphere, and improved dispersibility when the concentration reaches 10 wt%. A concentration of 10 wt% is an optimal choice for enhancing the spherical shape of the nano-microspheres.

Subsequently, to investigate the effects of different treatments on sc-PLA nano-microspheres, static and medium-low speed stirring treatments were employed during the phase



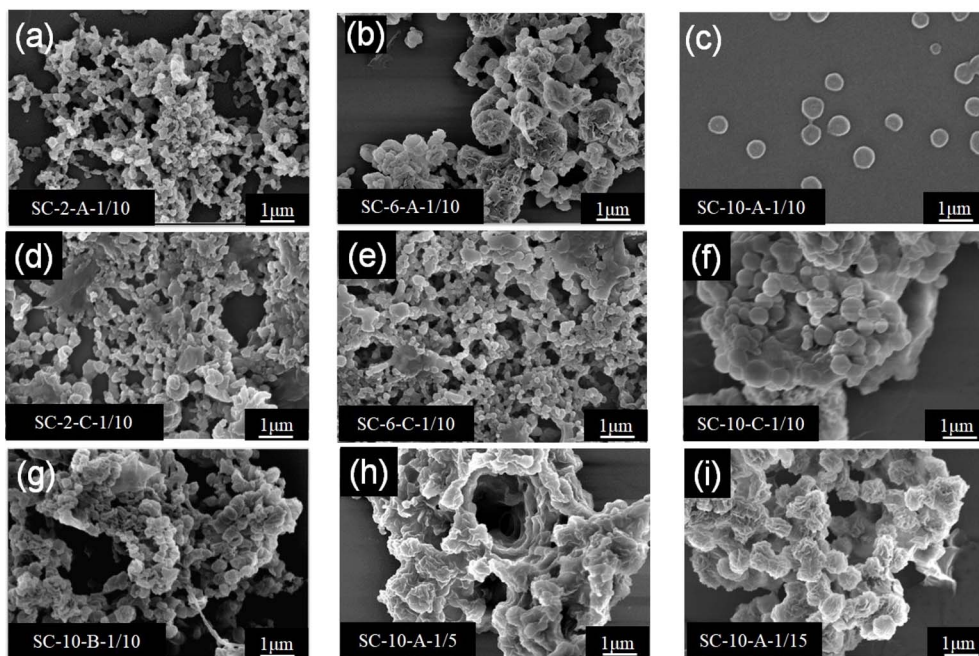


Fig. 2 SEM images of sc-PLA nano-microspheres: (a) SC-2-A-1/10, (b) SC-6-A-1/10, (c) SC-10-A-1/10, (d) SC-2-C-1/10, (e) SC-6-C-1/10, (f) SC-10-C-1/10, (g) SC-10-B-1/10, (h) SC-10-A-1/5, (i) SC-10-A-1/15.

separation process to separate the sc-PLA nano-microspheres. As shown in Fig. 2, the nano-microspheres obtained through static treatment (SC-10-A-1/10) were uniform in size and well-dispersed, while the nanoparticles obtained through stirring treatment (SC-10-B-1/10, SC-10-C-1/10) had smaller sizes, exhibited different dimensions, and were piled up together. Among them, when the concentration was 10%, the microsphere surfaces treated by low-speed stirring and static treatment were smoother, while the microsphere surfaces treated by medium-speed stirring remained rough. The higher the shear rate, the greater the shear force. This might be attributed to the effect of shear force, which damaged the surface morphology of the microspheres. Moreover, the MT solvent used for phase separation has a high polarity. The electron cloud density around the oxygen atom connected to the hydrocarbon group is large, and the binding force with hydrogen is strong. Therefore, MT is more likely to dissociate hydrogen. This solvation effect weakens the H-bonding in the stereoscopic crystal, thereby reducing the particle size. The microspheres tend to adhere and accumulate, resulting in an unsatisfactory phase separation effect.

Finally, to further compare the effects of different bath ratios on the morphology of nano-microspheres, as shown in Fig. 2, the nano-microspheres have the most regular morphology, consistent size, and homogeneous dispersion when the ratio of the PLLA/PDLA blend solution to the poor solvent used for phase separation is 1 : 10.

FTIR spectroscopy was used to demonstrate the successful preparation of the sc-PLA. It can be seen from Fig. 3 that the C=O stretching vibration peak of the ester functional group appears in the microspheres, which proves the existence of

stereoscopic crystals in the microspheres.<sup>45</sup> In addition, the infrared absorption peak attributed to sc-PLA is observed at  $908\text{ cm}^{-1}$ , assigned to the coupling of C-C backbone stretching with the  $\text{CH}_3$  rocking mode.<sup>46</sup> As shown in Fig. 3a, it can be observed that sc-PLA nano-microspheres can be successfully prepared from the mixture of the three different concentrations of the solution. The absorption peak of sc-PLA nano-microspheres prepared at 10 wt% (SC-10-A-1/10) is highest, indicating that the percentage of the stereo-complexed crystals is highest.

As shown in Fig. 3b, it can be observed that the sc-PLA nano-microspheres prepared in a static state (SC-10-A-1/10) exhibit a higher intensity of C=O peaks, whereas the sc-PLA nano-microspheres prepared in a stirred state (SC-10-B-1/10) exhibit lower peaks of the C=O telescoping vibration peaks due to the absence of the effect of the solution shear. The C=O telescoping vibration peaks of the SC-10-B-1/10 treatment are lower due to the absence of the effect of the solution shear. The C=O telescoping vibration peaks of the SC-10-A-1/10 treatment are not influenced by the solution shear force. The fact that without the effect of solution shear, the dipole moment changes of the SC-10-A-1/10's C=O stretching vibration peak is increased, resulting in an increase in absorption intensity, which gives rise to a strong and broad absorption peak. Moreover, the wave numbers of the characteristic peaks of SC-10-A-1/10 shifted to a lower position, indicating the formation of a greater number of H-bonding ( $\text{O}\cdots\text{H}$ ) interactions between the enantiomers of SC-10-A-1/10 and a stronger H-bonding effect. Fig. 3b illustrates that sc-PLA could be prepared by both preparation methods, and SC-10-A-1/10 has a higher percentage of sc-PLA. This is due to the polarity of the MT solution used for phase separation,



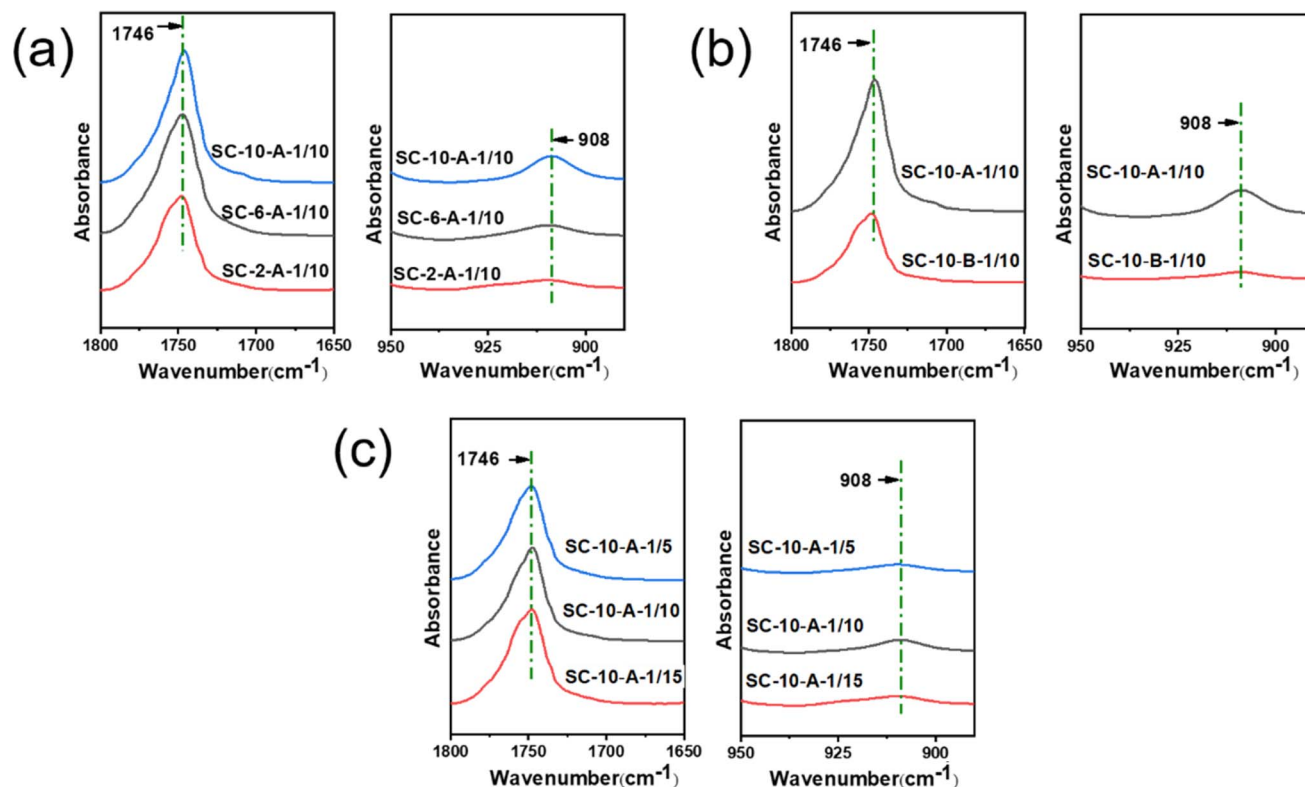


Fig. 3 FTIR images of sc-PLA nano-microspheres: (a) different concentrations: 2 wt%, 6 wt%, 10 wt%, (b) different treatments: stationary treatment, stirred treatment, (c) different ratios of blend solution to poor solvent: 1/5, 1/10, 1/15.

which produces a solvation effect, thereby weakening the H-bonding ( $O\cdots H$ ) between the enantiomers. Consequently, the stability of the stereo-complexed crystals reduced under shear, which affects the crystallinity of the stereo-complexation complex crystals. Finally, Fig. 3c indicates that varying bath ratios exert minimal influence on characteristic peaks, with minimal differences observed. To facilitate further comparison of the percentage of stereo-complexed crystals, the percentage of stereo-complexed crystals is determined by XRD test.

### 3.2. Crystallographic structure of the sc-PLA nano-microspheres

XRD shows the diffraction peaks of different crystal types of PLA. The diffraction peaks of the homo-crystallites were located near  $2\theta = 16.6^\circ$ . The crystals of sc-PLA belonged to the triclinic crystal system,<sup>47</sup> and the diffraction peaks were located near  $2\theta = 11.8^\circ$ ,  $20.6^\circ$  and  $23.8^\circ$ . As illustrated in Fig. 4a, the diffraction peaks of the stereo-complexed crystals exhibited a notable decline and then increase significantly as the solution concentration was gradually elevated. This phenomenon can be attributed to the fact that the molecular chain segments were able to attain their full extensibility at low concentrations, subsequently undergoing stereo-complexation through the formation of H-bonding. The diffraction peaks of the SC-10-A-1/10 stereo-complexed crystallites exhibited the highest intensity at a concentration of 10% PLA, while those of the homo-crystallites reached the lowest intensity. This observation is

likely the fact that with the concentration of PLA, the diffraction peaks were the highest. This is likely due to the increase in the number of macromolecular chains with the increase in concentration, which in turn promoted charge migration between the donor and the acceptor, accelerated H-bonding complexation, and promoted the molecular chains of the enantiomers to entangle with each other. Ultimately, this resulted in a significant increase in stereo-complexed crystal diffraction peaks.

As illustrated in Fig. 4b, the intensity of the diffraction peak of the stereo-complexed crystal of SC-10-A-1/10 is the highest and that of the homo-crystallite is nearly zero during the static phase separation. In contrast, a stronger diffraction peak of the homo-crystallite of the sample SC-10-B-1/10 emerged at  $16.6^\circ$  after the stirring treatment. The reason is that MT, the solvent used for phase separation, is polar and produces a solvation effect that weakens the H-bonding of  $O\cdots H$  in the stereo-complexed crystals. From the perspective of electron cloud analysis, the hydrocarbon group exerts a repulsive force on electrons, and the oxygen atom connected to the hydrocarbon group exhibits a high electron cloud density, resulting in a stronger bonding force with hydrogen. Consequently, MT is more likely to dissociate hydrogen atoms. The role of shear force in stirring treatment is also noteworthy. The greater the shear rate, the greater the shear force. The combined effect of shear force and polar solvent on the H-bonding ( $O\cdots H$ ) between enantiomers in the stereo-complexed crystal resulted in



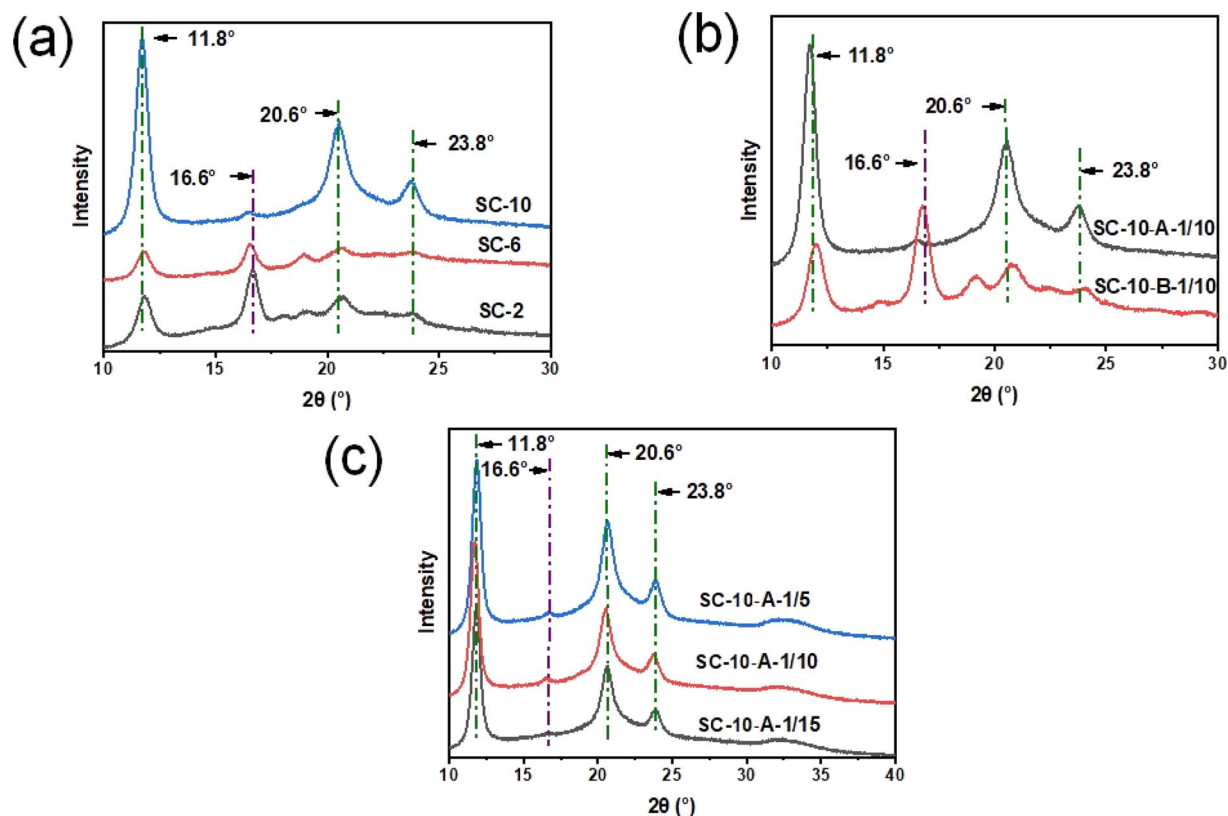


Fig. 4 XRD image of sc-PLA nano-microspheres: (a) different concentrations: 2 wt%, 6 wt%, 10 wt%, (b) different treatments: stationary treatment, stirred treatment, (c) different ratios of blend solution to poor solvent: 1/5, 1/10, 1/15.

a certain degree of damage, which subsequently led to a reduction in particle size. This also had a negative impact on the phase separation effect, as nano-microspheres were prone to adhesion and accumulation.

As illustrated in Fig. 4c, when the ratio of PLLA/PDLA blend solution to phase separation poor solvent is 1 : 5, 1 : 10, and 1 : 15, sc-PLA nano-microspheres exhibit robust diffraction peaks of stereo-complexed crystals at 11.8°, 20.6°, and 23.8°, with little difference in the intensities. The diffraction peaks of homo-crystallites are negligible at 16.6°. This suggests that the different bath ratios exert minimal influence on the percentage of stereo-complexed crystals.

As illustrated in Table 1, the highest degree of crystallinity was observed in stereo-complexed crystals, while the lowest degree of crystallinity was observed in homo-crystallites of SC-10-A-1/10. This was observed when the solution concentration

was 10%. Furthermore, the crystallization of stereo-complexed crystals reached a maximum of 99.65%. These findings provide empirical evidence to support the conclusions presented in Fig. 4. Consequently, to enhance the crystallinity of sc-PLA nano-microspheres, the optimal process parameter is a solution concentration of 10%. This conclusion is consistent with that of SEM and FTIR.

During the static phase separation, the SC-10-A-1/10 stereo-complex crystals exhibited the highest degree of crystallinity, the homo-crystallites exhibited the lowest degree of crystallinity, and the stereo-complexed crystals exhibited a degree of crystallinity of up to 99%. During the stirred phase separation, the stereo-complex crystals were partially destroyed due to the double effects of shear force and polar solvent. Consequently, the stereo-complex crystals of the SC-10-B-1/10 had a lower crystallinity, the homo-crystallites had a higher crystallinity, and the stereo-complexed crystals had a lower crystallinity. Furthermore, the crystallinity of SC-10-B-1/10 stereo-complexed crystallinity decreased, the crystallinity of homo-crystallites increased, and the rate of stereo-complexation also decreased. A comparison of the three sets of data reveals that the crystallinity of homo-crystallites increases with the decrease in the crystallinity of stereo-complexed crystals. This indicates that the stereo-complexed crystals and homo-crystallites are in competition with each other.

The crystallinity of stereo-complexed crystals, homo-crystallites, and the rate of stereo-complexed crystals of nano-

Table 1 Crystallinity of sc-PLA nano-microspheres

Sample	$X_{c,S}$ (%)	$X_{c,H}$ (%)	Rate of stereo-complexation (%)
SC-10-A-1/10	39.60	0.14	99.65
SC-6-A-1/10	7.40	0.51	93.55
SC-2-A-1/10	9.21	4.13	69.04
SC-10-B-1/10	14.12	10.86	56.53
SC-10-A-1/5	39.07	0.03	99.94
SC-10-A-1/15	39.10	0.11	99.72



microspheres exhibited minimal variation under different ratio of PLLA/PDLA blend solution to poor solvent. The highest crystallinity of stereo-complexed crystals was observed when the ratio of the PLLA/PDLA blend solution to the poor solvent used for phase separation was 1 : 10. This may be attributed to the fact that at all three ratios, the molecular chains can be effectively unfolded, thereby enabling efficient phase separation of the nano-microspheres. The highest degree of crystallinity was observed in stereo-complexed crystals when the ratio of the PLLA/PDLA blend solution to the poor solvent for phase separation was 1 : 10. As illustrated in Fig. 2c, the morphology of the sc-PLA nano-microspheres is most regular, which is optimal for combination with the stereo-complexed crystallinity presented in the Table 1.

### 3.3. Thermal performance of the sc-PLA nano-microspheres

Fig. 5 depicts the DSC curves of sc-PLA nano-microspheres prepared at varying solution concentrations with distinct treatments of phase separation solutions. The melting temperature at 220 °C was observed from the DSC heating curve in Fig. 5a, indicating the formation of stereo-complexed crystals in the nano-microspheres formed at all three concentration conditions. Among them, when the concentration condition was 10%, the melting absorption peak of nano-microspheres (SC-10-A-1/10) at 221 °C was higher than that of the other two concentrations, indicating a greater degree of stereo-complexation. In contrast, when the concentration conditions were 2% and 6%, the melt absorption peaks of nano-microspheres (SC-2-A-1/10, SC-6-A-1/10) appeared at 175 °C, indicating that homo-crystallites were formed in the nano-microspheres. In contrast, no homo-crystallite was generated in SC-10-A-1/10. As illustrated in Fig. 5b, the DSC heating curve revealed that SC-10-A-1/10 prepared under static conditions exhibited a melting temperature at 221 °C, with no discernible melting peak at 178 °C. This indicated the formation of stereo-complexed crystals, with the absence of homo-crystallites in SC-10-A-1/10. However, the sc-PLA nano-microspheres (SC-10-B-1/10) existed with melting points located near 170 °C and 210 °C under stirring conditions, indicating that both stereo-complexed crystals and homo-crystallites existed in SC-10-B-1/10/

10 under stirring conditions. Consequently, when the solution concentration is 10%, the phase-separated solution is in a static state, which is conducive to the generation of sc-PLA nano-microspheres.

### 3.4. Solvent stability of the sc-PLA nano-microspheres

As sc-PLA nano-microspheres would be utilized as drug carriers or materials in biomedical applications, sc-PLA nano-microspheres must exhibit certain stability and solvent resistance. Consequently, the solvent resistance of sc-PLA nano-microspheres must be considered during the preparation and application of sc-PLA nano-microspheres to ensure the morphology, structure, and stability of the nano-microspheres and thus the controlled release of drugs.

To observe the solvent resistance of the stereo-complexation PLA nano-microspheres, the sc-PLA nano-microspheres were immersed in CHL for 24 hours. As can be seen in Fig. 6a, the sc-PLA nano-microspheres were suspended and stabilized in CHL. The internal morphology of SC-10-A-1/10 was then observed by TEM. As shown in Fig. 6b, the stereo-complexed crystals are clearly seen to be stacked and agglomerated, which indicates that the stereo-complexation PLA nano-microspheres have better solvent resistance, but the edges are blurred due to the agglomeration phenomenon. This is due to the small polarity of CHL, which is unable to affect the strength of O···H hydrogen bonds between enantiomers in the stereo-complexed crystals. This also indicates that the linear structure of the cyclic chain between enantiomers, consisting of two O···H hydrogen bonds, is more stable.<sup>48</sup> Consequently, CHL is unable to dissolve the stereo-complexed crystals, and only the amorphous region of SA-10-A can be solubilized. Meanwhile, the pore-like structure witnessed in the background of Fig. 6b can be ascribed to the microporous organic membrane. Moreover, the microporous organic membrane is competent in providing a pore-like background in the TEM, which contributes to elevating the clarity and contrast of the sample imaging. In addition, by observing the surface morphology of SC-10-A-1/10 through SEM, its solvent resistance can be more comprehensively evaluated. As shown in Fig. 6c, the spherical shape of the PLA microspheres can be clearly observed again, but there are pits on the

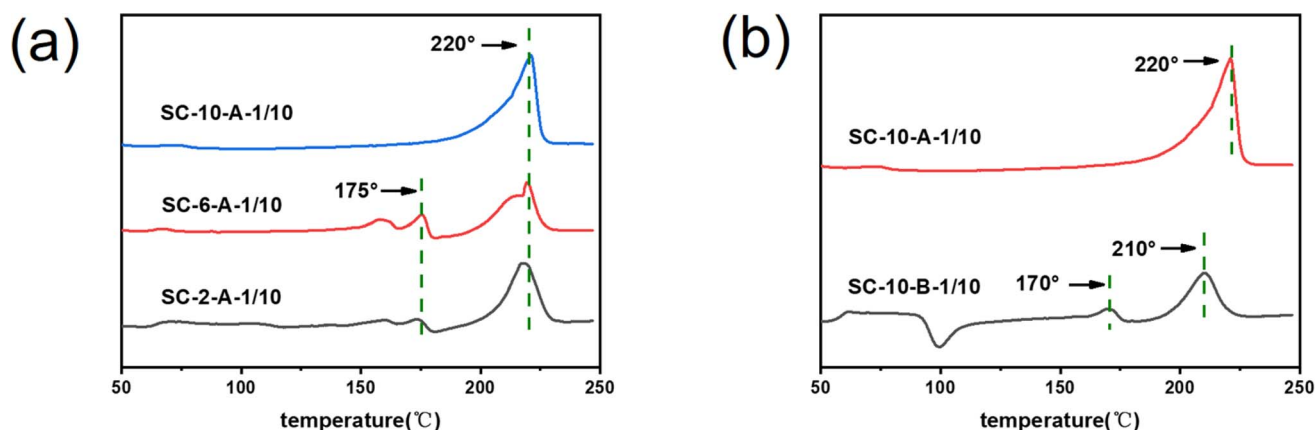


Fig. 5 DSC images of sc-PLA nano-microspheres: (a) different concentrations: 2 wt%, 6 wt%, 10 wt%, (b) different treatments: stationary, stirred.



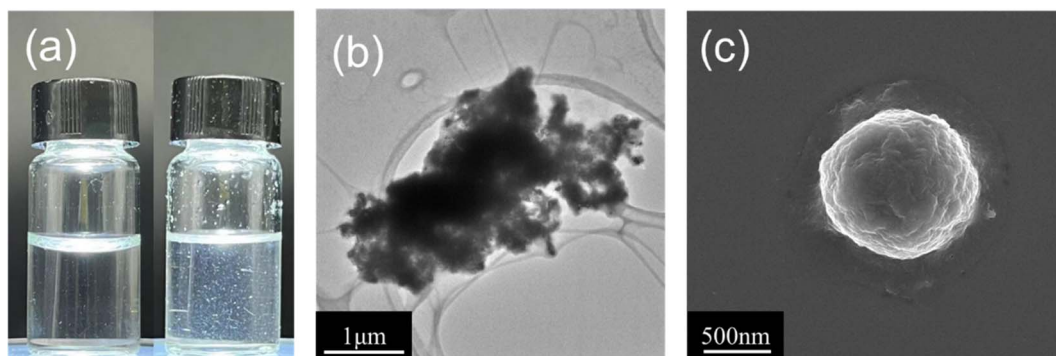


Fig. 6 Comparison of solvent resistance of sc-PLA nano-microspheres: (a) comparison of sc-PLA nano-microspheres placed in CHL immersion for 24 h, (b) TEM image of SC-10-A-1/10 after CHL immersion, (c) SEM image of SC-10-A-1/10 after CHL immersion.

surface wrinkles. This may be due to the fact that a fraction of amorphous region is dissolved by CHL, while the main body of the microsphere is not damaged due to the excellent solvent resistance of sc-PLA.

## 4 Conclusions

This research proposes a simple method for the preparation of sc-PLA nano-microspheres. The separation of sc-PLA nano-microspheres is achieved by adding a poor solvent to the phase separation of PLLA/PDLA blend. The effects of different process parameters (concentration, treatment, and the ratio of blend to poor solvents) on the morphology, crystallinity, and thermal properties of the nano-microspheres are investigated. It was demonstrated that when the concentration reached 10 wt% and the ratio of the blending solution to the poor solvent for phase separation was 1:10, the sc-PLA nano-microspheres exhibited greater regularity in shape, superior sphericity, and more homo-crystallites. What's more, the degree of crystallinity of the stereo-complexed crystals was as high as 39.60%, the rate of stereo-complexation was 99.65%, and the melting temperature reached 220 °C, indicating that the stereo-complexed crystals had the highest degree of crystallinity. Given this, it is clear that the crystallization and thermal properties of sc-PLA nano-microspheres had been significantly improved. Although the solvent phase separation method for preparing microspheres is simple and effective, there exist issues such as the dependence on specific solvents, solvent residues, size stability, and production efficiency. The future development direction should focus on the adoption of green solvents and the realization of large-scale production to address these problems. The successfully prepared sc-PLA nano-microspheres in this study exhibit superior thermal and crystallization properties and can serve as nucleating agents for fibers and carriers for drugs, further broadening their application scope in the medical, textile, and potentially other fields.

## Ethical statement

This article does not contain any studies with human participants or animals performed by any of the authors.

## Data availability

All the data and materials are accessible on request. Correspondence and requests for materials and data should be addressed to Ming Hua.

## Author contributions

Ming Hua: writing – original draft, methodology, investigation. Ying Pan: visualization, investigation, formal analysis. Changmei Jiang: methodology, investigation. Peiyan Yu: formal analysis. Xingang Li: methodology. Yao Gao: investigation. Sijun Xu: funding acquisition, formal analysis. Gangwei Pan: writing – review & editing, supervision, data curation.

## Conflicts of interest

The authors declare no competing financial interest.

## Acknowledgements

This work was supported by the “Pioneer” and “Leading Goose” Research and Development Program of Zhejiang (No. 2024C01185), Open Fund of State Key Laboratory of Biobased Fiber Manufacturing Technology (SKL202319), National Key Research and Development Program of China (2021YFC2600301), the Natural Science Foundation of the Higher Education Institutions of Jiangsu Province (23KJA540002) and Natural Science Foundation of Jiangsu Province (BK20190925, BK20200968). Authors also acknowledge the financial supports from the Key Research and Development Program of Jiangsu Province (BE2021025) and the China Postdoctoral Science Foundation (2021T140346).

## References

- 1 Y. Dong, Y. Xie, X. Ma, L. Yan, H. Yu, M. Yang, S. Abdalkarim and B. Jia, *Carbohydr. Polym.*, 2023, **321**, 121325.
- 2 A. P. Dove, *Chem. Commun.*, 2008, **48**, 6446–6470.
- 3 Y. Baimark, W. Rungseesantivanon and N. Prakymoramas, *Mater. Today Commun.*, 2022, **33**, 1–8.





- 4 S. Inkinen, M. Stolt and A. Södergård, *Biomacromolecules*, 2010, **11**, 1196–1201.
- 5 D. A. S. Marques, S. Jarmelo, C. M. S. G. Baptista and M. H. Gil, *Macromol. Symp.*, 2010, **296**, 63–71.
- 6 Y. Li, L. Chen, Y. Stehle, M. Lin, C. Wang, R. Zhang, M. Huang, Y. Li and Q. Zou, *J. Mater. Sci. Technol.*, 2024, **171**, 222–234.
- 7 S. Zhang, D. Yan, L. Zhao and J. Lin, *Compos. Commun.*, 2022, **34**, 101268.
- 8 T. A. M. Valente, D. M. Silva, P. S. Gomes, M. H. Fernandes, J. D. Santos and V. Sencadas, *ACS Appl. Mater. Interfaces*, 2016, **8**, 3241–3249.
- 9 M. Ekinici, C. C. Dos Santos, L. M. R. Alencar, H. Akbaba, R. Santos-Oliveira and D. Ilem-Ozdemir, *ACS Omega*, 2022, **7**, 47956–47966.
- 10 X. Chen, R. Zhang, Y. Mao and L. Zhong, *Chem. Eng. J. Adv.*, 2023, **467**, 143419.
- 11 L. Yan, S. Abdalkarim, X. Chen, Z. Chen, W. Lu, J. Zhu, M. Jin and H. Yu, *Compos. Sci. Technol.*, 2024, **245**, 110364.
- 12 S. Krishnan, P. Pandey, S. Mohanty and S. Nayak, *Polym.-Plast. Technol. Eng.*, 2016, **55**, 1623–1652.
- 13 Y. Li, H. Shen, S. Wang, H. Zhang, J. Hu, R. Xin and S. Yan, *Polymer*, 2023, **280**, 126037.
- 14 M. Guo, W. Wu, W. Wu and R. Wang, *Phys. Chem. Chem. Phys.*, 2023, **25**, 27.
- 15 D. Karst and Y. Yang, *Polymer*, 2006, **47**, 4845–4850.
- 16 D. Karst and Y. Yang, *Macromol. Chem. Phys.*, 2008, **209**, 168–174.
- 17 T. R. Cooper and R. F. Storey, *Macromolecules*, 2008, **41**, 655–662.
- 18 Z. Yan, Y. Wang, T. Li, P. Xu, J. Huang, J. Jiang, X. Zhang, B. Xia, S. Wang and W. Dong, *RSC Adv.*, 2022, **46**, 15064.
- 19 M. Guo, W. Wu, W. Wu, R. Wang, L. Huang and Q. Gao, *Phys. Chem. Chem. Phys.*, 2023, **25**, 17737–17758.
- 20 M. Fujita, T. Sawayanagi, H. Abe, T. Tanaka, T. Iwata, K. Ito, T. Fujisawa and M. Maeda, *Macromolecules*, 2008, **41**, 2852–2858.
- 21 B. Yu, L. Meng, S. Fu, Z. Zhao, Y. Liu, K. Wang and Q. Fu, *Colloids Surf., B*, 2018, **172**, 105–112.
- 22 L. Feng, X. Bian, G. Li and X. Chen, *Macromolecules*, 2022, **55**, 1709–1718.
- 23 S. Nouri, C. Dubois and P. G. Lafleur, *Polymers*, 2015, **67**, 227–239.
- 24 J. Sun, J. Shao, S. Huang, B. Zhang, G. Li, X. Wang and X. Chen, *Mater. Lett.*, 2012, **89**, 169–171.
- 25 J. Xu, Y. Li, Y. Li, Y. Chen, R. Wang, G. Liu, S. Liu, H. Ni and Z. Li, *Polymer*, 2018, **140**, 179–187.
- 26 S. Yang, G. Zhong, J. Xu and Z. Li, *Polymer*, 2016, **105**, 167–171.
- 27 B. Ma, H. Zhang, K. Wang, H. Xu, Y. He and X. Wang, *Compos. Commun.*, 2020, **21**, 1–6.
- 28 M. Guo, W. Wu, W. Wu and Q. Gao, *ACS Omega*, 2022, **7**, 41412–41425.
- 29 K. Chen, P. Chen, B. Qi, X. Zhang, L. Cao, C. Sun, H. Tan and Y. Zhang, *Composites, Part B*, 2024, **283**, 111663.
- 30 R. Guo, X. Sun, Y. Zhang, D. Wang, C. Yang and Z. Xu, *J. Colloid Interface Sci.*, 2018, **530**, 465–472.
- 31 J. Li, J. Wang, J. Li, X. Yang, J. Wan, C. Zheng, Q. Du, G. Zhou and X. Yang, *Acta Biomater.*, 2021, **131**, 532–543.
- 32 C. Xiao, X. Shen and L. Tao, *Int. J. Pharm.*, 2013, **452**, 227–232.
- 33 Y. Wu and R. Clark, *J. Colloid Interface Sci.*, 2007, **310**, 529–535.
- 34 M. Parhizkar, P. Reardon, J. Knowles, R. Browning, E. Stride, P. Barbara, A. Harker and M. Edirisinghe, *Nanomedicine*, 2016, **12**, 1919–1929.
- 35 C. Dharmayanti, T. Gillam, D. Williams and A. Blencowe, *Polymers*, 2020, **12**, 2930.
- 36 A. Cossé, C. König, A. Lamprecht and K. Wagner, *AAPS PharmSciTech*, 2017, **18**, 15–26.
- 37 D. Zhang, H. Zheng, K. Geng, J. Shen, X. Feng, P. Xu, Y. Duan, Y. Li, R. Wu, Z. Gou and C. Gao, *Biomaterials*, 2021, **272**, 120783.
- 38 H. Ribeiro, B. Chu, S. Ichikawa and M. Nakajima, *Food Chem.*, 2008, **22**, 12–17.
- 39 K. Mulia, G. Witkamp, G. Dawes, L. Fratila-Apachitei, I. Apachitei, J. Duszczek and H. Pellikaan, *J. Biomater. Appl.*, 2011, **25**, 401–412.
- 40 S. Bee, Z. Hamid, M. Mariatti, B. Yahaya, K. Lim, S. Bee and L. Sin, *J. Macromol. Sci., Polym. Rev.*, 2018, **58**, 495–536.
- 41 G. Whitesides, *Nature*, 2006, **442**, 368–373.
- 42 J. Zhai, Y. Wang, X. Zhou, Y. Ma and S. Guan, *J. Drug Delivery*, 2020, **27**, 1281–1291.
- 43 B. Li, H. Yang, K. Cheng, H. Song, J. Zou, C. Li, W. Xiao, Z. Liu and X. Liao, *Colloids Surf., B*, 2023, **223**, 113175.
- 44 Z. Feng, B. Zhou, X. Su, T. Wang, S. Guo, H. Yang and X. Sun, *Mater. Des.*, 2023, **225**, 11516.
- 45 M. Zhang, L. Chen, H. Yang and J. Ma, *J. Phys. Chem. A*, 2017, **121**, 4560–4568.
- 46 J. Zhang, K. Tashiro, H. Tsuji and A. Domb, *Macromolecules*, 2007, **40**, 1049–1054.
- 47 G. Pan, H. Xu, B. Ma, J. Wizi and Y. Yang, *J. Mater. Sci.*, 2018, **53**, 5490–5500.
- 48 T. Okihara, M. Tsuji, A. Kawaguchi, K. Katayama, H. Tsuji, S. Hyon and Y. Ikada, *J. Macromol. Sci., Part B: Phys.*, 1991, **30**, 119–140.

